Intramolecular Triplet Energy Transfer in Metal Polypyridine Complexes Bearing Ethynylated Aromatic Groups

Abdelkrim El-ghayoury,[†] Anthony Harriman,*[,‡] Abderrahim Khatyr,[†] and Raymond Ziessel[†]

Laboratoire de Chimie, d'Electronique et de Photonique Moléculaires, Ecole Européenne de Chimie, Polymères et Matériaux, Université Louis Pasteur, UPRES-A 7008 au CNRS, 25 rue Becquerel, 67087 Strasbourg Cedex 2, France, and Department of Chemistry, University of Newcastle, Newcastle upon Tyne NE1 7RU, United Kingdom

Received: August 25, 1999; In Final Form: November 24, 1999

A series of polytopic ligands has been synthesized in which a central aromatic hydrocarbon (1,4-phenylene, 1,4-naphthalene, or 9,10-anthracene) is linked to 2,2′-bipyridine (bpy) or 2,2′:6′,2″-terpyridine (terpy) units via ethynylene bonds and the coordination sites have been capped with one or two metal [M = Ru(II) or Os(II)] residues. The phenylene connector has little effect on the photophysical properties of the terminal metal complexes, except in the case of "Ru(terpy)" where the triplet lifetime is prolonged relative to the parent complex. An exceptionally long triplet lifetime ($\tau_T = 475$ ns) is found for the corresponding binuclear Ru(terpy)-based complex built around the naphthalene-derived connector, although the lowest-energy triplet state is associated with the metal complex. Reversible intramolecular triplet energy transfer occurs between the reactants in the "Ru(bpy)"-containing systems assembled from the naphthalene-based connector, with the lowest-energy triplet state being of naphthalene-like character. The photophysical properties of the corresponding "Os(bpy)" fragments remain relatively unaffected upon replacing phenylene with naphthalene. Fast triplet energy transfer occurs from the Ru(bpy) fragments to the central anthracene unit, the latter lying at much lower energy, but reversible triplet energy transfer is found with the Os(bpy) units linked to anthracene. The various rate constants for electron exchange are considered in terms of current theory to estimate a value for the matrix element ($V_{DA} \approx 8$ cm^{-1}). Triplet energy transfer from the Ru(bpy) fragments to anthracene falls well within the Marcus inverted region.

Introduction

Intramolecular triplet energy transfer has been studied extensively, especially for photoactive dyads containing at least one luminescent metal polypyridine complex[1] where the triplet state can be visualized by emission spectroscopy. In particular, ruthenium(II) tris(2,2′-bipyridine) complexes bearing pendant aryl hydrocarbons have been studied in some detail.[2−13] Thus, Ford and Rodgers[2] first observed reversible triplet energy transfer between a ruthenium(II) tris(polypyridine) complex and a covalently linked pyrene unit that extended the triplet lifetime of the metal complex from ≈1 to 11.2 μs in deoxygenated solution at room temperature. Subsequent work by Sasse et al.[3,4] and by Harriman et al.[5,6] has extended this field and shown that reversible triplet energy transfer between the metal complex and pyrene is a viable method for prolonging the triplet lifetime of the metallochromophore. In contrast, Schmehl and co-workers[7] found only weak electronic communication between triplet states localized on a ruthenium(II) tris(diimine) complex and on pyrene when linked by a single bond. Other studies have described triplet energy transfer from a metal complex to an aryl hydrocarbon[8−12] but, in several cases, the photosystems are unstable with respect to sensitized oxygenation of the polycycle.[8,9,11]

Most of the above studies employed photoactive dyads built around flexible connectors where rates of intramolecular energy transfer cannot be separated from the effects of diffusion. In fact, there is a scarcity of kinetic data relating to triplet energy transfer in such dyads.[14] We now describe the results of a spectroscopic investigation of the energy-transfer processes occurring in sterically constrained dyads in which an aryl hydrocarbon is attached to a metal polypyridine complex via an ethynylene group.[15] In each case, the aromatic hydrocarbon is at the center of a polytopic ligand so that both mono- and binuclear complexes can be studied. So as to vary the relative triplet energies, both ruthenium(II) and osmium(II) complexes have been used while, in some cases, the 2,2′-bipyridyl coordination sites have been replaced with 2,2′:6′,2″-terpyridyl units. An obvious extension of this work involves the construction of mixed-metal Ru−Os complexes where triplet energy transfer occurs along the molecular axis.[15] As such, the most interesting systems are those for which triplet states localized on the bridging aromatic hydrocarbon possess energy levels between those of the metal polypyridine complexes so that energy transfer might take place via a two-step mechanism.[16] The main purpose of the present investigation, therefore, is to identify the most appropriate molecular fragments from which to construct useful multicomponent architectures. In this respect it should be noted that the ethynylene substituents have a marked and variable influence on the triplet energy levels of the various subunits.

Experimental Section

Materials. The techniques and apparatus used to characterize all new compounds are detailed elsewhere.[17] Synthesis of the various polytopic ligands has been reported previously.[18]

* To whom correspondence should be addressed.
[†] Université Louis Pasteur.
[‡] University of Newcastle.

10.1021/jp9930447 CCC: $19.00
Published on Web 01/27/2000

Preparation of the complexes was realized by reaction of the free ligand with a stoichiometric amount of the metal precursor: (i) with bpy as the chelating unit $[Ru(bpy)_2Cl_2]\cdot 2H_2O$[19] or $[Os(bpy)_2Cl_2]$[20] was used in deoxygenated ethanol, under overnight reflux; (ii) with terpy as the chelating unit $[Ru(terpy)(dmso)Cl_2]$[21] was previously dehalogenated with $AgBF_4$ in methanol and allowed to react with the free ligand in deoxygenated methanol at 80 °C overnight. The precursor $[Os(terpy)O_2(OH)](NO_3)$[22] was used in a tetrahydrofuran/water mixture containing hydrazine at 50 °C for 22 h. In each case, the course of reaction was followed by thin-layer chromatography. At the completion of reaction, excess KPF_6 in water was added and the organic solvent slowly evaporated on a rotavapor. The dark-red solid was isolated by centrifugation, washed with water, and the residue loaded onto a neutral alumina column and eluted with dichloromethane using a 0−20% gradient of methanol. In general, the first fraction was discarded and the subsequent highly colored band was collected. Recrystallization from acetone/hexane afforded the required complex in an analytically pure state. Satisfactory yields were obtained in each case and the isolated complexes were characterized by various spectroscopic techniques as follows.

RBP. Yield: 60% (R_f = 0.55, alumina, CH_2Cl_2/CH_3OH: 95/5, v/v). UV/vis (CH_3CN): λ_{max}, nm (ϵ, M^{-1} cm^{-1}) 281 (74,100), 446 (11 000). IR (KBr pellets): 2924 (w), 2219 (w, $\nu_{C\equiv C}$), 1596 (w), 1460 (m), 843 (s). ES-MS: *m/z* 424.1 $\{M\text{-}2PF_6\}^{2+}$. Anal. Calcd. for $C_{50}H_{34}N_8RuP_2F_{12}$ (M_r = 1138.123): C, 52.72; H, 3.01, N, 9.84. Found: C, 52.53; H, 2.69; N, 9.53.

OBP. Yield: 75% (R_f = 0.50, alumina, CH_2Cl_2/CH_3OH: 95/5, v/v). UV/vis (CH_3CN): λ_{max}, nm (ϵ, M^{-1} cm^{-1}) 284 (87 500), 357 (71 700), 448 (12 600). IR (KBr pellets): 2221 (w, $\nu_{C\equiv C}$), 1590 (w), 1462 (m), 1267 (w), 843 (s). ES-MS: *m/z* 468.4 $\{M\text{-}2PF_6\}^{2+}$. Anal. Calcd. for $C_{50}H_{34}N_8OsP_2F_{12}$ (M_r = 1228.181): C, 48.85; H, 2.79; N, 9.12. Found: C, 48.63; H, 2.51; N, 8.83.

RBPBR. Yield: 40% (R_f = 0.22, alumina, CH_2Cl_2/CH_3OH: 95/5, v/v). UV/vis (CH_3CN): λ_{max}, nm (ϵ, M^{-1} cm^{-1}) 280 (123 000), 323 (52 000), 357 (65 100), 444 (20 000). IR (KBr pellets): 2926 (w), 2855 (w), 2223 (w, $\nu_{C\equiv C}$), 1601 (w), 1465 (m), 839 (s) cm^{-1}. ES-MS: *m/z* 469.4 $\{M\text{-}3PF_6\}^{3+}$, 776.3 $\{M\text{-}2PF_6\}^{2+}$. Anal. Calcd. for $C_{70}H_{50}N_{12}Ru_2P_4F_{24}$ (M_r = 1842.092): C, 45.60; H, 2.74; N, 8.32. Found: C, 45.53; H, 2.69; N, 8.24.

OBPBO. Yield: 50% (R_f = 0.40, alumina, CH_2Cl_2/CH_3OH: 95/5, v/v). UV/vis (CH_3CN): λ_{max}, nm (ϵ, M^{-1} cm^{-1}) 283 (136 400), 359 (80 300), 449 (22 800). IR (KBr pellets): 2925 (w), 2224 (w, $\nu_{C\equiv C}$), 1641 (w), 1464 (m), 841 (s) cm^{-1}. ES-MS: *m/z* 528.7 $\{M\text{-}3PF_6\}^{3+}$, 865.2 $\{M\text{-}2PF_6\}^{2+}$. Anal. Calcd. for $C_{70}H_{50}N_{12}Os_2P_4F_{24}$ (M_r = 2022.209): C, 41.54; H, 2.49; N, 8.31. Found: C, 41.39; H, 2.35; N, 8.23.

RTPTR. Yield: 51% (R_f = 0.40, alumina, CH_3CN/toluene: 80/20, v/v). UV/vis (CH_3CN): λ_{max}, nm (ϵ, M^{-1} cm^{-1}) 271 (86 600), 308 (125 400), 494 (54 700). IR (KBr pellets): 2925 (w), 2213 (w, $\nu_{C\equiv C}$), 1634 (w), 1612 (m), 1448 (m), 1385 (s), 840 (s) cm^{-1}. FAB^+ (m-NBA): 1693.2 $[M\text{-}PF_6]^+$, 1549.2 $[M\text{-}2PF_6 + H]$, 1403.3 $[M\text{-}3PF_6]^+$. Anal. Calcd. for $C_{70}H_{46}N_{12}Ru_2P_4F_{24}\cdot CH_3CN$ (M_r = 1837.224 + 41.053): C, 46.04; H, 2.63; N, 9.69. Found: C, 45.94; H, 2.52; N, 9.55.

RBN. Yield: 60% (R_f = 0.53, alumina, CH_2Cl_2/CH_3OH: 95/5, v/v). UV/vis (CH_3CN): λ_{max}, nm (ϵ, M^{-1} cm^{-1}) 280 (83 100), 450 (12 100), 470 (9 100). IR (KBr pellets): 2924 (w), 2206 (w, $\nu_{C\equiv C}$), 1593 (w), 1456 (m), 1241 (w), 843 (s) cm^{-1}. ES-MS: *m/z* 449.5 $\{M\text{-}2PF_6\}^{2+}$, 1043.5 $\{M\text{-}PF_6\}^+$. Anal. Calcd. for $C_{54}H_{36}N_8RuP_2F_{12}$ (M_r = 1188.139): C, 54.60; H, 3.05; N, 9.43. Found: C, 54.30; H, 2.72; N, 9.13.

OBN. Yield: 60% (R_f = 0.57, alumina, CH_2Cl_2/CH_3OH: 95/5). UV/vis (CH_3CN): λ_{max}, nm (ϵ, M^{-1} cm^{-1}) 284 (83 100), 385 (56 700), 470 (12 000). IR (KBr pellets): 2206 (w, $\nu_{C\equiv C}$), 1593 (w), 1460 (m), 1273 (w), 843 (s). ES-MS: *m/z* 494.8 $\{M\text{-}2PF_6\}^{2+}$, 1133.2 $\{M\text{-}PF_6\}^+$. Anal. Calcd. for $C_{54}H_{36}N_8OsP_2F_{12}$ (M_r = 1278.197): C, 50.70; H, 2.84; N, 8.76. Found: C, 50.54; H, 2.40; N, 8.39.

RBNBR. Yield: 40% (R_f = 0.21, alumina, CH_2Cl_2/CH_3OH: 95/5, v/v). UV/vis (CH_3CN): λ_{max}, nm (ϵ, M^{-1} cm^{-1}) 280 (143 200), 450 (25 200), 470 (19 400). IR (KBr pellets): 2924 (w), 2210 (w, $\nu_{C\equiv C}$), 1600 (w), 1445 (m), 841 (s) cm^{-1}. ES-MS: *m/z* 486.0 $\{M\text{-}3PF_6\}^{3+}$, 801.3 $\{M\text{-}2PF_6\}^{2+}$. Anal. Calcd. for $C_{74}H_{52}N_{12}Ru_2P_4F_{24}$ (M_r = 1892.108): C, 46.93; H, 2.77; N, 8.88. Found: C, 46.71; H, 2.38; N, 8.53.

OBNBO. Yield: 40% (R_f = 0.25, alumina, CH_2Cl_2/CH_3OH: 95/5, v/v). UV/vis (CH_3CN): λ_{max}, nm (ϵ, M^{-1} cm^{-1}) 290 (136 000), 446 (29 800), 470 (22 800). IR (KBr pellets): 2925 (w), 2209 (w, $\nu_{C\equiv C}$), 1625 (w), 1464 (m), 840 (w). ES-MS: *m/z* 545.4 $\{M\text{-}3PF_6\}^{3+}$, 890.3 $\{M\text{-}2PF_6\}^{2+}$, 1925.1 $\{M\text{-}3PF_6\}^+$. Anal. Calcd. for $C_{74}H_{52}N_{12}Os_2P_4F_{24}$ (M_r = 2072.223): C, 42.85; H, 2.53; N, 8.11. Found: C, 42.72; H, 2.27; N, 8.18.

RTN. Yield: 33%. (R_f = 0.26, alumina, $CH_3CN/H_2O/KNO_3$ sat. in water 80/16/4, v/v/v). UV/vis (CH_3CN): λ_{max}, nm (ϵ, M^{-1} cm^{-1}) 272 (70 500), 308 (75 900), 389 (29 400), 510 (40 800). IR (KBr pellets): 2960 (w), 2926 (m), 2854 (w), 2208 (w, $\nu_{C\equiv C}$), 1694 (w), 1452 (m), 1262 (w), 1029 (m), 843(s) cm^{-1}. ES-MS: *m/z* 486.9 $\{M\text{-}2PF_6\}^{2+}$. Anal. Calcd. for $C_{59}H_{37}N_9RuP_2F_{12}\cdot CH_3CN$ (M_r = 1263.011+ 41.052): C, 56.18; H, 3.09; N, 10.74. Found: C, 55.86; H, 2.82; N, 10.56.

RTNTR. Yield: 31% (R_f = 0.42, alumina, $CH_3CN/H_2O/KNO_3$ sat. in water 80/16/4, v/v/v). UV/vis (CH_3CN): λ_{max}, nm (ϵ, M^{-1} cm^{-1}) 281 (95 600), 308 (70 300), 393 (59 200), 513 (87 100). IR (KBr pellets): 2203 (w, $\nu_{C\equiv C}$), 1649 (m), 1630 (m), 1607 (m), 1474 (w), 1419 (w), 1028 (m), 842 (s) cm^{-1}. Anal. Calcd. for $C_{74}H_{48}N_{12}RuP_2F_{12}\cdot CH_3CN$($M_r$ = 1887.284 + 41.052): C, 47.34; H, 2.67; N, 9.44. Found: C, 47.18; H, 2.44; N, 9.27.

RBA. Yield: 50% (R_f = 0.63, alumina, CH_2Cl_2/CH_3OH: 95/5, v/v). UV/vis (CH_3CN): λ_{max}, nm (ϵ, M^{-1} cm^{-1}) 276 (61 000), 328 (21 800), 457 (24 000). IR (KBr pellets): 2924 (w), 2197 (w, $\nu_{C\equiv C}$), 1604 (w), 1464 (m), 1241 (w), 843 (s) cm^{-1}. ES-MS: *m/z* 474.0 $\{M\text{-}2PF_6\}^{2+}$. Anal. Calcd. for $C_{58}H_{38}N_8RuP_2F_{12}$ (M_r = 1238.155): C, 56.27; H, 3.09; N, 9.05. Found: C, 55.89; H, 2.87; N, 8.64.

OBA. Yield: 50% (R_f = 0.55, alumina, CH_2Cl_2/CH_3OH: 95/5, v/v). UV/vis (CH_3CN): λ_{max}, nm (ϵ, M^{-1} cm^{-1}) 283 (83 300), 328 (38 400), 457 (44 900). IR (KBr pellets): 2924 (w), 2191 (w, $\nu_{C\equiv C}$), 1593 (w), 1459 (m), 842 (s) cm^{-1}. ES-MS: *m/z* 518.5 $\{M\text{-}2PF_6\}^{2+}$. Anal. Calcd. for $C_{58}H_{38}N_8OsP_2F_{12}$ (M_r = 1328.213): C, 52.49; H, 2.88; N, 8.44. Found: C, 52.19; H, 2.53; N, 8.09.

RBABR. Yield: 40% (R_f = 0.28, alumina, CH_2Cl_2/CH_3OH: 95/5, v/v). UV/vis (CH_3CN): λ_{max}, nm (ϵ, M^{-1} cm^{-1}) 279 (146 600), 466 (41 700), 500 (3 100). IR (KBr pellets): 2908 (w), 2203 (w, $\nu_{C\equiv C}$), 1699 (w), 1600 (w), 1466 (s), 1445 (m), 1241 (w), 834 (s) cm^{-1}. ES-MS: *m/z* 340.4 $\{M\text{-}4PF_6\}^{4+}$, 502.1 $\{M\text{-}3PF_6\}^{3+}$, 825.6.4 $\{M\text{-}2PF_6\}^{2+}$. Anal. Calcd. for $C_{78}H_{54}N_{12}Ru_2P_4F_{24}$ (M_r = 1942.124): C, 48.19; H, 2.80; N, 8.65. Found: C, 48.03; H, 2.63; N, 8.41.

Methods. Absorption spectra were recorded at ambient temperature with a Kontron Instruments Uvikon 930 spectrophotometer. Luminescence spectra were recorded in deoxygen-

ated acetonitrile at 20 °C using a modified Perkin-Elmer LS50 spectrofluorimeter equipped with a silicon photocell as the detector operated at 77 K. The emission monochromator was replaced so as to allow data to be collected from 500 to 1000 nm and the resultant spectra were corrected for imperfections of the instrument by reference to a standard lamp. Spectra were averaged over 10 runs and the quoted emission maxima were reproducible to within ±5 nm. Quantum yields were calculated relative to ruthenium(II) and osmium(II) tris(2,2′-bipyridyl) complexes in acetonitrile,[23,24] using dilute solutions after deoxygenation by purging with argon. Luminescence quantum yields were taken as the average of three separate determinations and were reproducible to within ±8%. For the various metal complexes, the excitation source was a mode-locked argon ion laser emitting at 514 nm. To record excitation spectra, the argon ion laser was replaced with the conventional Xe lamp supplied with the LS50. The same lamp was used as the excitation source for the free polytopic ligands.

Luminescence lifetimes were measured using two different instruments. For long-lived emission, the sample was illuminated with a 25-ps laser pulse at 532 nm as delivered by a frequency-doubled, mode-locked Nd:YAG laser. For some studies, the excitation pulse was Raman-shifted with perdeuterated cyclohexane to produce excitation wavelengths of 598 or 465 nm. The laser intensity was attenuated to 5 mJ/pulse and incident pulses were defocused onto an adjustable pinhole positioned in front of the sample cuvette. Luminescence was collected with a microscope objective lens at 90° to excitation and isolated from any scattered laser light with nonemissive glass cutoff filters. The emergent luminescence was focused onto the entrance slit of a Spex high-radiance monochromator and thereby passed to a fast-response photomultiplier tube. The output signal was transferred to a Tektronix SCD1000 transient recorder and subsequently to a microcomputer for storage and analysis. Approximately 500 individual laser shots, collected at 10 Hz, were averaged for kinetic measurements. The temporal resolution of this instrument was ≈2 ns. Emission lifetimes measured with this setup were reproducible to within ±5%. All kinetic measurements were made with samples previously deoxygenated by purging with argon and the absorbance of each solution was adjusted to be ≈0.08 at the excitation wavelength. Data analysis was made by a nonlinear, least-squares iterative fitting routine that utilized a modified Levenberg−Marquardt global minimization procedure, after deconvolution of the instrument response function.[25]

For shorter-lived emission, the lifetime was measured by time-correlated, single-photon counting techniques using a frequency-doubled Ti sapphire laser (Spectra Physics, Tsunami, 880 nm) operated at a repetition rate of 82 MHz. Emission was collected at right angles, using the setup described above, and directed to a fast response microchannel plate phototube operated at low temperature. The luminescence decay data were fit to the sum of two exponentials by iteratively convoluting trial decay curves with the instrumental response function generated by scattering the laser pulse with a suspension of latex particles. Decay curves were collected at 12 different emission wavelengths and on 4 different time scales before being analyzed by global methodology. The temporal resolution of this setup was ≈25 ps.

Transient differential absorption spectra were recorded after excitation of the sample in deoxygenated acetonitrile with a 25-ps laser pulse at 532 nm. Where appropriate, the excitation pulse was Raman-shifted with perdeuterated cyclohexane to produce excitation wavelengths of 598 and 465 nm or frequency-tripled to 355 nm. The monitoring beam was provided by a pulsed, high-intensity Xe arc lamp passed through the sample at 90° to the excitation pulse. Spectra were compiled point-by-point, with five individual records being collected at each wavelength, using a Spex high-radiance monochromator operated with 2-nm slits. Kinetic measurements were made at a fixed wavelength, with 100 individual laser shots being averaged for each decay profile. The time resolution of this setup was restricted to ≈2 ns by the rise time of the PMT but was improved to ≈50 ps by replacing the Xe monitoring beam with a pulse of white light generated by focusing residual laser light into a mixture of D_2O/H_2O. The excitation pulse was delayed with respect to that of the continuum with a computer-controlled optical delay stage and the two pulses were directed almost collinearly through the sample cell. The continuum pulse was split 50/50 before the sample cell so as to provide sample and reference beams. After passing through the sample, these beams were collected by fiber optics and analyzed with an image-intensified, Princeton dual-diode array spectrograph. The spectrometer was operated at 10 Hz, with 100 individual laser shots being averaged at each delay time. Baseline corrections were applied and emission was subtracted from the resultant spectra by recording control signals without the excitation or continuum pulses. Differential absorption spectra were corrected for distortions by reference to the optical Kerr effect obtained from CS_2.

Improved time resolution was achieved using a frequency-doubled, mode-locked Antares 76S pumped dual-jet dye laser operated with either pyromethene (565 nm) or Rhodamine 6G (600 nm) dyes. The output beam was split into two parts with ≈80 and 20% of the total intensity, respectively. The most intense beam was used as the excitation source (fwhm = 350 fs) while the weaker beam was depolarized and focused into a 1-cm cuvette filled with water to produce a white light continuum for use as the analyzing pulse. The continuum was split into two equal beams before reaching the delay stage so as to provide a reference beam by which to normalize the transient absorption spectrum. This reference beam arrived at the sample cell ≈1 ns before the excitation and analyzing beams, with the latter two pulses passing almost collinearly through the sample. Detection and data analysis was made as mentioned above. Additional studies were made with a frequency-doubled, Q-switched Nd:YAG laser (fwhm = 15 ns) using the facilities available at the Paterson Institute for Cancer Research, Manchester, England.

Curve fitting of corrected emission spectra followed the procedure introduced by Meyer and co-workers.[12] Briefly, luminescence spectra recorded for the various reference compounds were corrected for spectral distortions of the instrument, reduced so as to display L/ν^3 versus ν where L is the luminescence intensity at wavenumber ν, and normalized. Each spectrum was deconvoluted into the minimum number of Gaussian-shaped bands needed to give a good representation of the complete spectrum using the commercially available PEAKFIT program. From the individual Gaussian components it was possible to identify (i) the energy difference between 0,0 vibronic levels in the triplet and ground states (E_0), (ii) the average half-width at half-maximum ($\Delta\nu_{1/2}$) for the series of bands, and (iii) the average energy spacing between individual vibronic bands ($\hbar\omega$). Subsequently, the entire emission spectrum was constructed using MATHCAD V6 and compared to the experimental spectrum using SCIENTIST to refine the parameters and to estimate the size of the electron-vibrational coupling constant S. PM3 RHF-SCF MO calculations for the S_0 and T_1 levels of the polytopic ligands were made with the MOPAC93 program package. For the configuration interaction calculations

TABLE 1: Cyclic Voltammetry Data Collected for the Various Compounds in Deoxygenated *N,N*-Dimethylformamide Containing Tetra-*N*-butylammonium Hexafluorophosphate (0.1 M)[a]

compound	$\nu_{C\equiv C}$ (cm^{-1})	E_{OX}	$E_{RED}(1)$	$E_{RED}(2)$	$E_{RED}(3)$	$E_{RED}(4)$
$[Ru(bpy)_3]^{2+}$	NA	1.30 (1e)	−1.25 (1e)	−1.52 (1e)	−1.79 (1e)	NA
RBP	2219	1.34 (1e)	−1.02 (1e)	−1.35 (1e)	−1.53 (1e)	−1.66 (1e)
RBPBR	2223	1.34 (2e)	−1.02 (2e)	−1.36 (2e)	−1.59 (2e)	NA
RBN	2206	1.34 (1e)	−0.99 (1e)	−1.31 (1e)	−1.41 (1e)	−1.64 (1e)
RBNBR	2210	1.34 (2e)	−0.97 (2e)	−1.35 (2e)	−1.57 (2e)	−1.88 (1e)
RBA	2197	1.35 (1e)	−0.91 (1e)	−1.11 (1e)	−1.37 (1e)	−1.61 (1e)
RBABR	2203	1.34 (2e)	−0.85 (2e)	−1.33 (2e)	−1.56 (2e)	−1.71 (1e)
$[Os(bpy)_3]^{2+}$	NA	0.83 (1e)	−1.25 (1e)	−1.54 (1e)	−1.80 (1e)	NA
OBP	2221	0.89 (1e)	−0.99 (1e)	−1.28 (1e)	−1.53 (1e)	−1.68 (1e)
OBPBO	2224	0.89 (2e)	−1.01 (2e)	−1.29 (2e)	−1.58 (2e)	NA
OBN	2206	0.90 (1e)	−0.96 (1e)	−1.26 (1e)	−1.40 (1e)	−1.63 (1e)
OBNBO	2209	0.90 (2e)	−0.94 (2e)	−1.28 (2e)	−1.48 (2e)	−1.60 (1e)
OBA	2192	0.88 (1e)	−0.92 (1e)	−1.12 (1e)	−1.31 (2e)	−1.56 (2e)

[a] Reduction potentials are in units of V vs SCE while the number of electrons associated with each process is given in parentheses. Also listed are the frequencies of the C≡C stretching vibration measured for KBr pellets.

of the T_1 state, the two highest occupied (HOMO and HOMO-1) and two lowest unoccupied (LUMO and LUMO+1) orbitals were taken into consideration. Ab initio MO calculations were made at the CIS/3-21G level after energy minimization of the structure using the AMBER force field.

Cyclic voltammetry studies were performed in deoxygenated *N,N*-dimethylformamide containing ammonium hexafluorophosphate (0.1 M) as the background electrolyte. The working and counter electrodes were constructed from Pt wires while a saturated calomel electrode (SCE) was used as the reference. The cell was calibrated by reference to ferrocene as the internal standard. Reduction potentials were reproducible to within ±10 mV. In all cases, the peaks were quasi-reversible with the peak currents for forward and reverse steps being equal, within experimental limits.

Results and Discussion

Background. The main purpose of this investigation is to explore the effect of a central aromatic unit on the photophysical properties of butadiynylene-linked binuclear [M = Ru(II) or Os(II)] polypyridine complexes. A separate study will concentrate on how this spacer unit influences the rate of intramolecular triplet energy transfer in the corresponding mixed-metal Ru−Os complexes.[26] Consequently, a set of polytopic ligands was designed[18] having a central 1,4-phenylene, 1,4-naphthalene, or 9,10-anthracene unit and with terminal 2,2′-bipyridine ligands as the coordinating sites. To assist interpretation of the photophysical results, a few additional compounds were synthesized having terminal 2,2′:6′,2″-terpyridine ligands. The abbreviations used throughout this manuscript can be explained as follows: The metal center is specified as being R [ruthenium(II)] or O [osmium(II)], with the overall charge being neglected. The coordinating ligand is either 2,2′-bipyridine [B] or 2,2′:6′,2″-terpyridine [T] while the central aromatic unit is selected from 1,4-phenylene [P], 1,4-naphthalene [N], or 9,10-anthracene [A]. For the binuclear complexes, all five structural units are specified (e.g., RBPBR) but only three units are given for the mononuclear complexes (e.g., RBP). In the latter case, the vacant ligand is the same as the coordinated ligand. The counteranion is hexafluorophosphate in each case. The polytopic ligands are identified by their three constituent units (e.g., BPB).

The alkynylene group is intended to fulfill several critical roles, in addition to providing structural integrity. First, because of its powerful electron-withdrawing effect, the ethynylene group will shift the reduction potential (E_{RED}) for the substituted ligand to a less negative value.[27] In turn, this ensures that the lowest-energy excited triplet state associated with the metal complex will be formed by selective charge injection from the metal center to the substituted ligand. Second, interaction between the ligand and substituent allows electron delocalization over an extended π^* orbital at the triplet level,[28] which stabilizes the triplet state.[29] Finally, the alkynylene group is an excellent conduit for electrons[30] and is likely to facilitate fast intramolecular electron exchange between the various subunits.[31] With regard to mechanistic considerations the ability of the alkynylene group to direct charge into the polytopic ligand is clearly a key feature that requires confirmation. Consequently, cyclic voltammetry studies were made in *N,N*-dimethylformamide to ascertain the effect of the substituent on the electrochemistry of the various metal complexes.

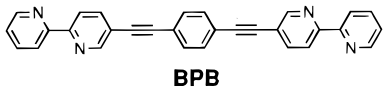

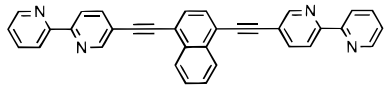

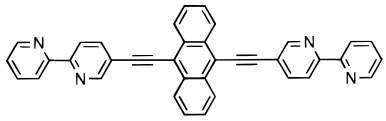

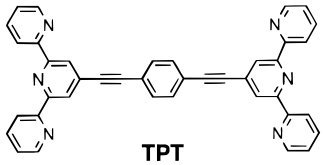

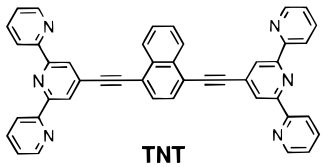

The substituent has little, if any, effect on the potential at which the metal center undergoes one-electron oxidation (E_{OX}) while, for the binuclear complexes, these metal centers are not strongly coupled (Table 1). For each mononuclear complex, it is apparent that the first electron is added to the coordinated

TABLE 2: Photophysical Properties and Spectroscopic Parameters Determined for the Phenylene-Bridged Metal Complexes and Ditopic Ligands in Deoxygenated Acetonitrile at 20 °C

compound	λ_L (nm)	Φ_L	τ_T (ns)	E_0 (cm^{-1})	λ_T (cm^{-1})	E_T (cm^{-1})	$\hbar\omega$ (cm^{-1})	S
$[Ru(bpy)_3]^{2+}$	627	0.062	980	15 950	1100	16 950	1380	0.75
RBP	650	0.056	905	15 330	1240	16 570	1300	0.95
RBPBR	653	0.050	820	15 300	1270	16 570	1310	0.84
$[Ru(terpy)_2]^{2+}$	650	<0.0001	0.56	15 330	950	16 280	1400	0.66
RTPTR	685	0.0006	110	14 600	800	15 400	1390	0.60
$[Os(bpy)_3]^{2+}$	745	0.0046	60	13 400	950	14 350	1390	0.71
OBP	790	0.0014	22	12 530	1045	13 575	1350	0.77
OBPBO	790	0.0012	19	12 500	1070	13 570	1340	0.78
BPB[a]	NA[b]	NA	NA	21 650	320	21 970	1300	0.25
TPT[a]	NA	NA	NA	21 110	290	21 400	1325	0.23

[a] Measured in micellar media at 20 °C. [b] NA means data not available.

end of the polytopic ligand because the first reduction potential ($E_{RED}(1)$) is significantly less negative than that of the relevant parent complex (Table 1). In most mononuclear complexes, the second electron is added to one of the parent ligands but because $E_{RED}(2)$ is less negative than that for the parent and is only slightly shifted from the parent $E_{RED}(1)$, it is clear that the first electron is delocalized over the alkynylene group. For the phenylene-bridged mononuclear complexes, the third ($E_{RED}(3)$) and fourth ($E_{RED}(4)$) electrons, respectively, are added to parent and polytopic ligands. However, for the naphthalene-bridged mononuclear complexes the third electron goes to the polytopic ligand while the fourth electron goes to the remaining parent ligand. With the anthracene-based mononuclear complexes, the second electron is added to the vacant end of the polytopic ligand, with the third and fourth electrons going to the parent ligands. The mononuclear 2,2′:6′,2″-terpyridine-based systems behave similarly except there is only one parent ligand. It is apparent that as the size of the central aromatic unit increases, there is a progressive shift toward less negative potentials for the E_{RED} associated with both complexed and vacant terminals of the polytopic ligand (Table 1).

With the various binuclear complexes, the first two electrons are added simultaneously to the polytopic ligand (Table 1). Again, there are strong indications for partial electron delocalization over the alkynylene group but because each terminal is reduced at the same potential, it is clear that the central aromatic unit plays the role of an insulator. Additional two-electron reduction steps can be attributed to successive reduction of the parent ligands, while for the naphthalene- and anthracene-based binuclear complexes the central aromatic unit is itself reduced at more negative potentials. The central unit exerts a strong effect on $E_{RED}(1)$ because it lowers the LUMO energy of the terminal coordination sites. In all cases, however, it is clear that the most easily reduced ligand is that bearing the ethynylene substituent.

Further evidence for electronic interaction between the ethynylene group and the central aromatic unit is available from infrared spectra recorded for solid-state samples. Here, the frequency found for the C≡C stretching vibration ($\nu_{C\equiv C}$) shifts progressively toward lower energy as the size of the central aromatic unit increases (Table 1). This effect is apparent for both mono- and binuclear complexes, regardless of the identity of the cation, and corresponds to a significant electronic perturbation.

Photophysical Properties of the Phenylene-Bridged Systems. The photophysical properties recorded for the various mono- and binuclear "Ru(bpy)"- and "Os(bpy)"-containing compounds remain similar to those measured for the parent complexes (Table 2). Absorption transitions due to the polytopic ligand appear in the UV region, making important contributions between 300 and 400 nm, but do not overlap to any significant

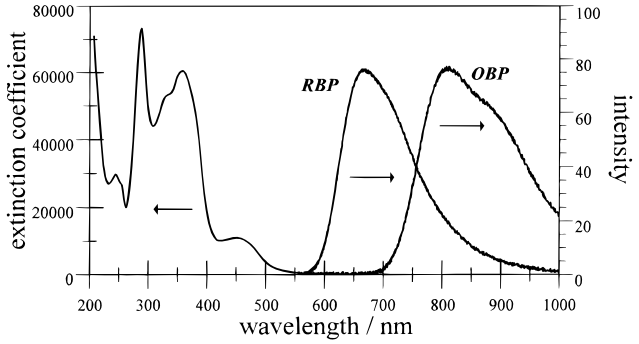

Figure 1. Absorption spectrum recorded for RBP in acetonitrile with the extinction coefficient having units of M^{-1} cm^{-1}. Also shown are normalized luminescence spectra recorded for RBP and OBP in deoxygenated acetonitrile at 20 °C.

degree with the metal-to-ligand, charge-transfer (MLCT) absorption bands associated with the metal complexes (Figure 1). The intense π,π^* transition associated with the parent 2,2′-bipyridine ligands is seen at 288 nm. In each case, the luminescence characteristic of the metal complex can be observed in deoxygenated acetonitrile at 20 °C (Figure 1), for which the quantum yield (Φ_L) and peak maximum (λ_L) are in the expected range. Emission decay profiles follow exponential kinetics, allowing determination of the triplet lifetime (τ_T), while the corrected excitation spectra remain in good agreement with the corresponding absorption spectra. For each compound, identical triplet lifetimes were measured by transient absorption spectrophotometry and by time-resolved emission spectroscopy, regardless of excitation or monitoring wavelength. Differential triplet absorption spectra recorded after laser excitation at 532 nm (Figure 2) indicate that the polytopic ligand is bleached during population of the triplet state, but this is to be expected if the triplet is formed by selective charge transfer from the metal center to the ethynylated ligand. No other species was observed in the spectral records and, as found in emission studies, the transient absorption signal decays cleanly to the prepulse baseline via exponential kinetics.

The situation is slightly different for the "Ru(terpy)"-based compound RTPTR where the triplet lifetime and emission probability greatly exceed those recorded for the parent complex (Table 2). However, this behavior is normal for an alkyne-substituted Ru(terpy) complex[32] and the photophysical properties recorded for RTPTR are as expected. The luminescence decay profile followed exponential kinetics while the corrected excitation spectrum remained in excellent agreement with the absorption spectrum, even in the region where the polytopic ligand dominates the spectral pattern. The differential triplet absorption spectrum shows clearly that the MLCT band associated with the metal center is bleached during triplet population (Figure 3a).

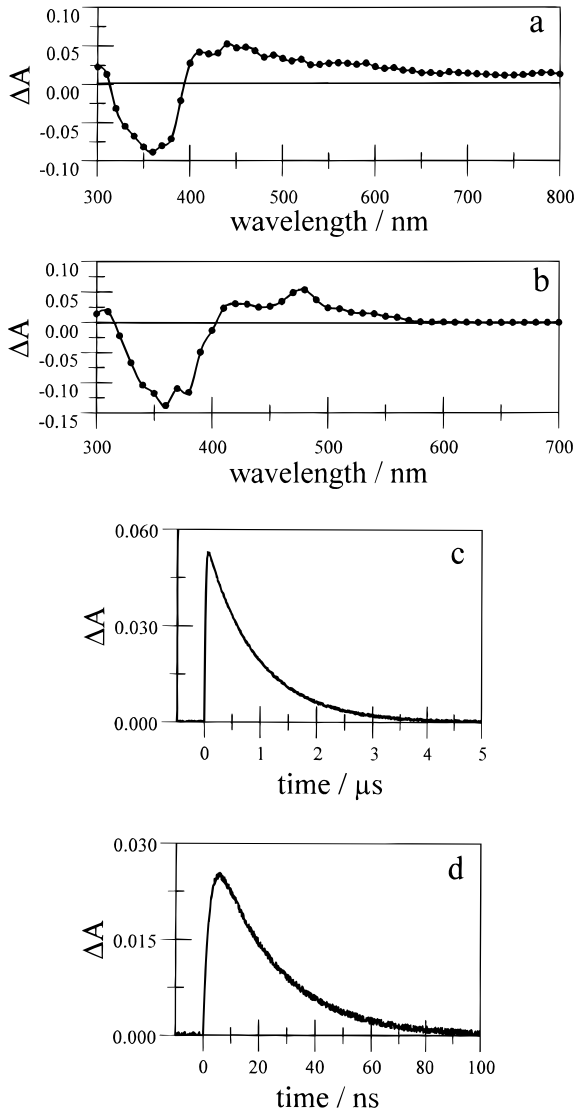

Figure 2. Triplet differential absorption spectra recorded for (a) RBP and (b) OBP following excitation at 532 nm with a 25-ps laser pulse. The spectra were recorded 10 ns after excitation. Also shown are decay profiles recorded at 440 nm for (c) RBP and (d) OBP in deoxygenated acetonitrile.

The triplet energy (E_T) of each chromophore was determined by the procedure of Meyer and co-workers.[12] Thus, the reduced emission spectrum[33,34] was deconstructed into the minimum number of Gaussian-shaped components of equal half-width ($\Delta\nu_{1/2}$). The peak maximum (E_0) of the highest-energy Gaussian is taken to represent the energy difference between 0,0 vibronic levels in the triplet and ground states while the energy spacing between adjacent Gaussian components ($\hbar\omega$) is attributed to the averaged medium-frequency vibrational mode coupled to the MLCT triplet state. The derived parameters were used to reconstruct the reduced luminescence spectrum according to[12]

$$L(\nu) = \sum_{x=0}^{5}\left[\left(\frac{E_0 - x\hbar\omega}{E_0}\right)^3\left(\frac{S^x}{x!}\right)\times \left(\exp\left[-4\ln 2\left(\frac{\nu - E_0 + x\hbar\omega}{\Delta\nu_{1/2}}\right)^2\right]\right)\right] \quad (1)$$

where the summation was restricted to $x = 5$. Iteration was continued until good agreement was reached between observed and calculated spectra, allowing refinement of the parameters

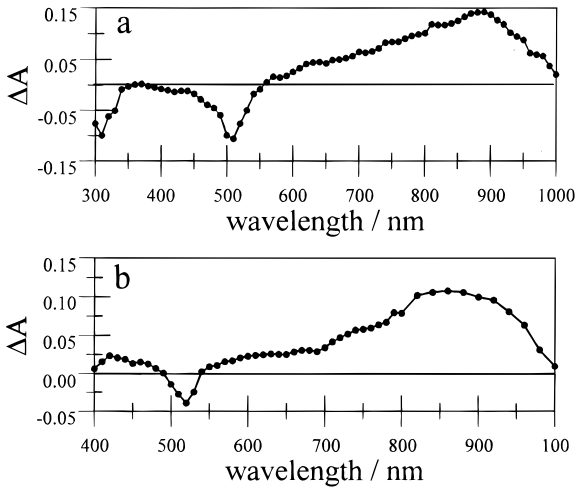

Figure 3. Triplet differential absorption spectra recorded for (a) RTP and (b) RTN following excitation at 532 nm with a 25-ps laser pulse. The spectra were recorded 10 ns after excitation.

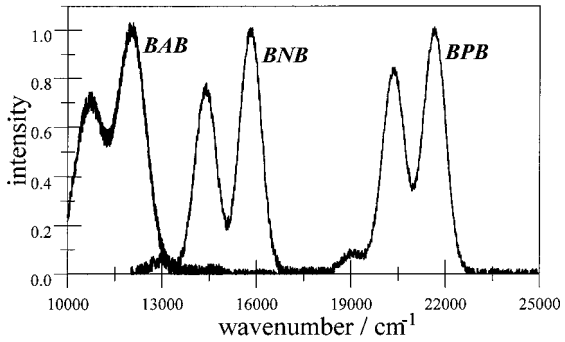

Figure 4. Phosphorescence spectra recorded for the 2,2′-bipyridyl-based polytopic ligands in deoxygenated micellar media at 20 °C. Each spectrum is the average of 100 individual records.

and calculation of the electron-vibrational coupling constants (S). The reorganization energy (λ_T) for each triplet, assumed to contain contributions from both nuclear and solvent terms, was estimated from the temperature ($-20 < T < 60$ °C) dependence of the half-width of the Gaussian components according to

$$\lambda_T = \frac{(\Delta\nu_{1/2})^2}{16k_B T\ln(2)} \quad (2)$$

while the triplet energy (E_T) was calculated as follows:

$$E_T = E_0 + \lambda_T \quad (3)$$

A complete listing of the derived parameters is given in Table 2.

Also included in Table 2 are the spectroscopic parameters determined for the polytopic ligands in micellar media[35] at room temperature (Figure 4a). Triplet energies derived for these ligands lie well above those of the corresponding metal complexes while the reorganization energies are relatively small.[36] Taken together with the modest S factors,[37] these findings indicate that the lowest-energy triplet states localized on the polytopic ligands are essentially π,π^* in character. Except for spectral broadening, these phosphorescence spectra are similar to those reported[38] for other alkynes in frozen glasses at 77 K and, in particular, the triplet energies appear to be within the expected range. Indeed, the experimental triplet energies are well-supported by MO calculations[39] made at the CIS/3-21G level because the two sets of values agree to within a

TABLE 3: Photophysical Properties and Spectroscopic Parameters Determined for the Naphthalene- and Anthracene-Bridged Metal Complexes and Ditopic Ligands in Deoxygenated Acetonitrile at 20 °C

compound	λ_L (nm)	Φ_L	τ_T (ns)	E_0 (cm^{-1})	λ_T (cm^{-1})	E_T (cm^{-1})	$\hbar\omega$ (cm^{-1})	S
RBN	656	0.035	7500	15 240	1165	16 405	1400	0.76
RBNBR	661	0.031	6700	15 120	1200	16 320	1440	0.83
RTN	696	0.0020	415	14 320	900	15 220	1360	0.66
RTNTR	702	0.0026	475	14 210	820	15 050	1380	0.60
OBN	800	0.0014	18	12 475	910	13 385	1350	0.67
OBNBO	805	0.0010	14	12 400	900	13 300	1350	0.70
RBA	670	<0.0001	7100	15 000	1300	16 300	1380	0.72
RBABR	680	<0.0001	5800	14 800	1520	16 320	1400	0.70
OBA	800	0.0021	415	12 250	900	13 150	1400	0.64
BNB[a]	NA[b]	NA	NA	15 810	290	16 100	1420	0.20
BAB[a]	NA	NA	NA	12 070	330	12 400	1400	0.36
TNT[a]	NA	NA	NA	16 390	310	16 700	1400	0.26

[a] Measured in micellar media at 20 °C. [b] NA means data not available.

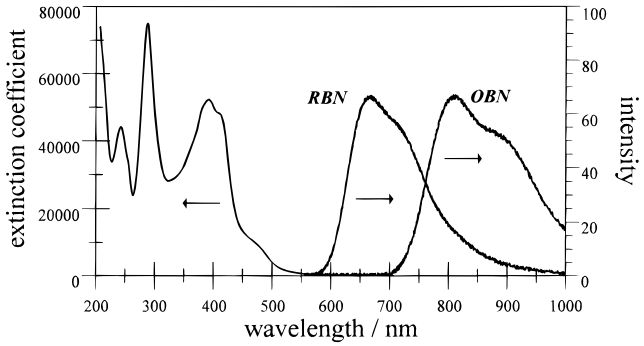

Figure 5. Absorption spectrum recorded for RBN in acetonitrile with the extinction coefficient having units of M^{-1} cm^{-1}. Also shown are normalized luminescence spectra recorded for RBN and OBN in deoxygenated acetonitrile at 20 °C.

few hundred cm^{-1}. It is now possible to assign the lowest-energy triplet in the phenylene-based systems as that localized on the terminal metal complex. In each case, the triplet associated with the connector lies at too high energy to interact significantly with that of the metal complex.

Photophysical Properties of the Naphthalene-Bridged Systems. Similar measurements were made for the various complexes built from the naphthalene-based polytopic ligands and the main results are collected in Table 3. For these systems, the polytopic ligand absorbs strongly in the range 300−450 nm and partially obscures MLCT transitions associated with the terminal metal complexes (Figure 5). It is possible, however, to ensure selective excitation of the metal complex by using longer wavelength (λ > 520 nm) irradiation. No fluorescence from the connector is detectable upon excitation at 380 nm and, for each complex, there is excellent agreement between corrected excitation and absorption spectra when monitoring emission from the metal complex. Thus, energy transfer from the connector to the terminal metal complex is quantitative. For each system, luminescence characteristic of the terminal metal complex is seen in deoxygenated acetonitrile at 20 °C (Figure 5). In fact, replacing the central phenylene fragment with naphthalene has only a minor effect on the photophysical properties of the Os-based complexes[12b,20,40] and it is clear that the lowest-energy triplet state remains localized on the metal complex. Decay profiles are exponential, in each case, while differential triplet absorption spectra (Figure 6) are consistent with the lowest-energy triplet state being resident on the metal complex. Relative to the corresponding phenylene-based complexes, there is a small red shift to the emission maximum and

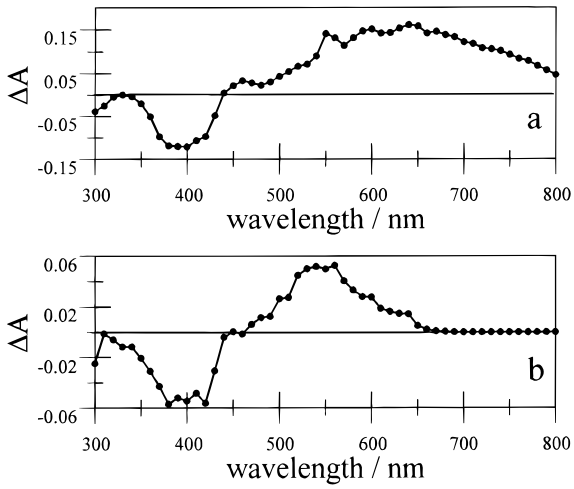

Figure 6. Triplet differential absorption spectra recorded for (a) RBN (fwhm = 15 ns; 532 nm; delay time, 50 ns) and (b) OBN (fwhm = 25 ps; 598 nm; delay time, 10 ns) following laser excitation.

a slight lowering of the triplet energy. This effect is attributed to improved blending of LUMOs localized on the terminals and on the connecting naphthalene residue[41] because the latter LUMO lies closer in energy to that of the terminals than is the case with a phenylene connector.[42] One consequence of this interaction is that the triplet energy of the metal complex is lowered and, in line with the energy-gap law,[36] the triplet lifetime is shortened.[40]

The photophysical properties of the Ru-based chromophores are changed markedly on replacing the central phenylene unit with naphthalene (Table 3). For the Ru(terpy)-based fragments there is a modest red-shift to the emission peak, a substantial increase in emission probability, and a significant prolongation of the triplet lifetime. Similar effects have been observed for an Ru(terpy) unit covalently linked to pyrene via an ethynylene group[5,6] and explained in terms of increased electron delocalization over an extended π^* orbital at the triplet level. Small differences between the mono- and binuclear complexes RTN and RTNTR are consistent with this idea. For both RTN and RTNTR, emission decay profiles remain exponential and the lifetimes are identical to those measured by transient absorption spectroscopy. In these latter studies, the differential triplet absorption spectra show extensive bleaching of the MLCT transition associated with the Ru(terpy) fragments (Figure 3b), indicating that the lowest-energy triplet state is that localized on the metal complex.

Replacing the central phenylene unit with naphthalene has serious consequencies for the Ru(bpy)-based chromophores present in RBN and RBNBR. In both cases, the emission peak undergoes a small red shift while the emission probability is decreased by almost 50%. There is a substantial increase in the triplet lifetime, as measured by both time-resolved emission spectroscopy and transient absorption spectrophotometry. In fact, despite the lower triplet energy, the triplet lifetimes of RBN and RBNBR exceed that of the parent complex, in apparent contradiction to the energy-gap law.[36] Differential triplet absorption spectra recorded for RBN and RBNBR (Figure 6) closely resemble that measured for the polytopic ligand and the obvious indication is that, in these complexes, the lowest-energy triplet state is that localized on the connector. However, because only the metal complex emits in deoxygenated acetonitrile, it follows that there must be thermal equilibration between triplets localized on the Ru(bpy) terminals and on the connector. Such behavior has been described previously for Ru(bpy) fragments covalently bound to pyrene.[2−6]

TABLE 4: Parameters Relating to Reversible Triplet Energy Transfer in the Naphthalene- and Anthracene-Based Metal Complexes, as Measured in Deoxygenated Acetonitrile at 20 °C

compound	K	ΔE_{TT} (cm^{-1})	k_{ET}^{F} (ns^{-1})	k_{ET}^{R} (ns^{-1})	τ_S (ps)	τ_T (μs)	FC (10^{-4} cm)[a]	V_{DA} (cm^{-1})[b]	k_M (μs^{-1})
RBN	4.5	305	10.9	2.4	75	8.6	0.66 (0.15)	11.8 (11.6)	1.1
RBNBR	3.0	220	9.0	3.0	83	6.7	0.50 (0.17)	12.3 (12.2)	1.2
RBA	NA	3900	12.0	NA	83	5.5	1.86	7.4	NA
RBABR	NA	3750	10.5	NA	90	5.5	1.98	6.7	NA
OBA	40	750	29.0	0.73	33	0.42	1.69 (0.04)	12.0 (11.9)	90

[a] Franck−Condon factor calculated for the forward reaction from the spectroscopic data listed in Table 3. The value in parentheses refers to the corresponding reverse energy-transfer process. [b] Matrix element for electron exchange calculated for the forward reaction. The value in parentheses is for the corresponding reverse energy-transfer step.

These spectroscopic studies require that the triplet energies of the naphthalene-based polytopic ligands lie close to those determined for the Ru(bpy) and Ru(terpy) fragments (Table 3). In fact, weak phosphorescence could be detected for both BNB and TNT in micellar media at room temperature so that the triplet energies can be measured independent of the kinetic studies. From the phosphorescence spectra (Figure 4b), it appears that the triplet energy of BNB is ≈300 cm^{-1} below that of RBN and 220 cm^{-1} below that of RBNBR while the triplet energy of TNT is ≈1500 cm^{-1} above that of RTNTR. These values appear to be consistent with the kinetic results and are in good agreement with triplet energies calculated by MO theory.[39] However, they differ markedly from the triplet energy of naphthalene (E_T = 21 300 cm^{-1})[43] but this is to be expected in view of the increased π-electron conjugation. Related molecular systems with naphthalene residues attached to Ru(bpy) fragments either directly[7] or via saturated connectors[3,4] have not shown reversible triplet energy transfer between the terminals. In such systems, as with RTNTR, the energy gap is too large to support reverse energy transfer and it is only in the special cases of RBN and RBNBR that the energetics are appropriate for reversible energy transfer.

Examination of the luminescence properties of RBN and RBNBR with improved temporal resolution shows, in both cases, a short-lived component to the decay profiles (Figure 7). This rapidly decaying signal accounts for ≈70% of the initial signal and corresponds to triplet lifetimes (τ_S) of 75 and 83 ps, respectively, for RBN and RBNBR. It possesses the same spectral profile as that recorded for the longer-lived component. The other naphthalene-based systems do not show this fast component in the decay profiles and, on this basis, it is attributed to intramolecular triplet energy transfer from the Ru(bpy) unit to the naphthalene-based connector. Because of the limited temporal resolution of the detector, it was not possible to obtain an accurate determination of the fractional contribution that this short-lived component makes to the total emission signal. Instead, we can estimate equilibrium constants (K) from the spectroscopic energy levels[44] and use these values, in conjunction with the measured τ_S values, to derive rate constants for forward (k_{ET}^{F}) and reverse (k_{ET}^{R}) energy-transfer steps (Table 4).

According to the derived equilibrium constants, the fraction (α) of the Ru(bpy) triplet present in the equilibrium mixture is 0.18 and 0.25, respectively, for RBN and RBNBR. Deactivation of these equilibrium mixtures occurs slowly via first-order kinetics. Assuming that the rates of equilibration greatly exceed the rate of deactivation, the measured rate constant ($k_M = 1/\tau_T$) for triplet decay can be expressed in terms of decay rates for the individual triplets

$$k_M = \alpha k_R + (1 - \alpha)k_N \qquad (4)$$

where k_R and k_N, respectively, refer to first-order rate constants for deactivation of the triplet states localized on Ru(bpy) and on the connector. Setting k_N equal to the rate constant measured for the polytopic ligand ($k_N = 3.0 \times 10^4\ s^{-1}$) allows estimation of k_R as being $(5.5 \pm 1.0) \times 10^5\ s^{-1}$. This estimate is comparable to rates measured for other ethynylated Ru(bpy) units.[28]

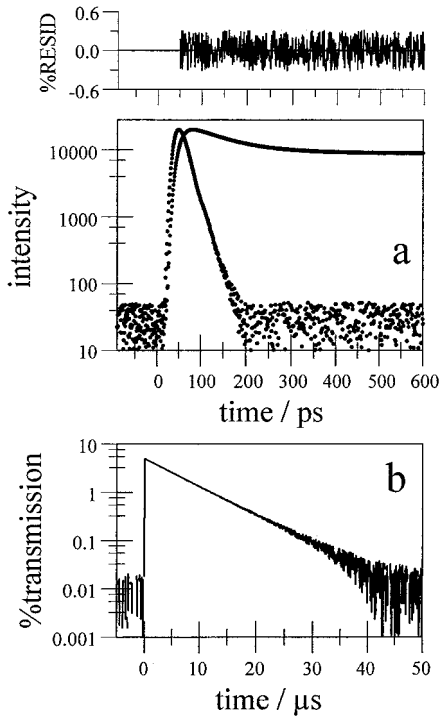

Figure 7. Time-resolved emission profile recorded at 660 nm after laser excitation (fwhm = 0.32 ps, 440 nm) of RBN in deoxygenated acetonitrile using single-photon counting methodology. Also shown is the instrument response function (IRF) and a computer-generated fit (χ^2 = 1.04) to the sum of two-exponential components (A_1 = 0.80, τ_S = 85 ps; A_2 = 0.20, τ_T = 1 μs) after deconvolution of the IRF. A plot of the weighted residuals is shown above the experimental decay curve. Note that the lifetime of the longer-lived component cannot be measured properly on this time scale. (b) Time-resolved luminescence profile recorded at 660 nm following excitation of RBN in deoxygenated acetonitrile with a 25-ps laser at 532 nm. The trace corresponds to the average of 100 individual records. The rise time of the PMT detector is ≈2 ns.

Photophysical Properties of the Anthracene-Bridged Systems. The anthracene-containing polytopic ligand absorbs strongly in the 400−530-nm region and overlaps MLCT transitions associated with the metal complexes (Figure 8). Fluorescence from the anthracene unit is completely quenched when the terminal metal complexes are in place. The Ru(bpy) fragments present in RBA and RBABR emit very weakly in deoxygenated acetonitrile at 20 °C (Figure 8) while differential transient absorption spectra are identical to that measured for the polytopic ligand BAB (Figure 9). Triplet decay profiles recorded for RBA and RBABR follow exponential kinetics, with the derived lifetimes remaining similar to that found for the

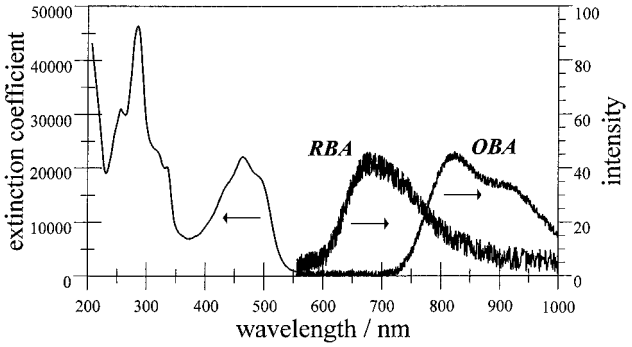

Figure 8. Absorption spectrum recorded for RBA in acetonitrile with the extinction coefficient having units of M^{-1} cm^{-1}. Also shown are normalized luminescence spectra recorded for RBA and OBA in deoxygenated acetonitrile at 20 °C.

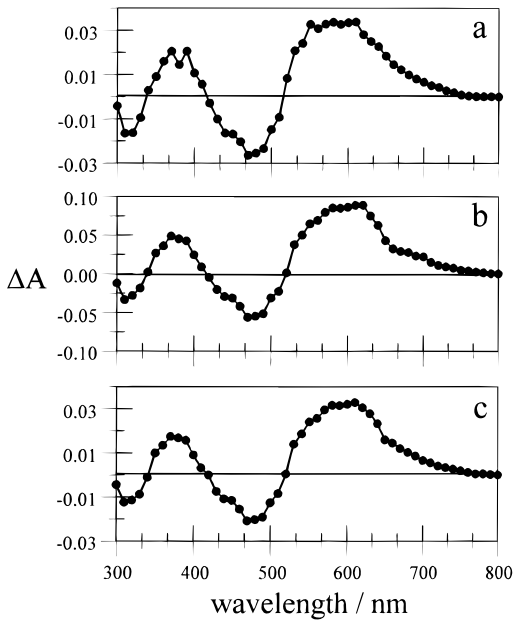

Figure 9. Triplet differential absorption spectra recorded for (a) RBA (fwhm = 15 ns; 532 nm; delay time, 50 ns) and (b) OBA (fwhm = 25 ps; 598 nm; delay time, 50 ns) following laser excitation. Panel (c) shows the corresponding spectrum recorded for BAB (fwhm = 25 ps; 355 nm; delay time, 100 ns).

polytopic ligand (Table 3). The triplet energy measured for BAB by room temperature phosphorescence in micellar media (Figure 4c) is significantly lower than those found for the corresponding Ru(bpy) fragments such that the lowest-energy triplet state in RBA and RBABR is that localized on the connector. Similar conclusions have been reached for other molecular dyads comprising Ru(bpy) and anthracene units[3,4,11] and it is clear that the anthracene triplet acts as an energy sink for photons absorbed by the Ru(bpy) fragment. It should be noted that, as for the other polytopic ligands, the triplet energy of BAB (E_T = 12 400 cm^{-1}) is much lower than that of the unsubstituted polycycle (E_T = 14 900 cm^{-1}),[43] although it is in good agreement with that calculated by MO theory (E_T = 11 900 cm^{-1}).[39]

Excitation of RBA with a subpicosecond laser pulse at 565 nm, where the Ru(bpy) fragment is the sole chromophore, generates the triplet state localized on the metal complex. This species decays rapidly via first-order kinetics to produce the differential absorption spectrum already assigned to the triplet state localized on the anthracene-based connector (Figure 10). Although the spectral changes occurring on the picosecond time scale are modest, a reliable estimate of the rate constant for intramolecular energy transfer can be obtained by averaging data

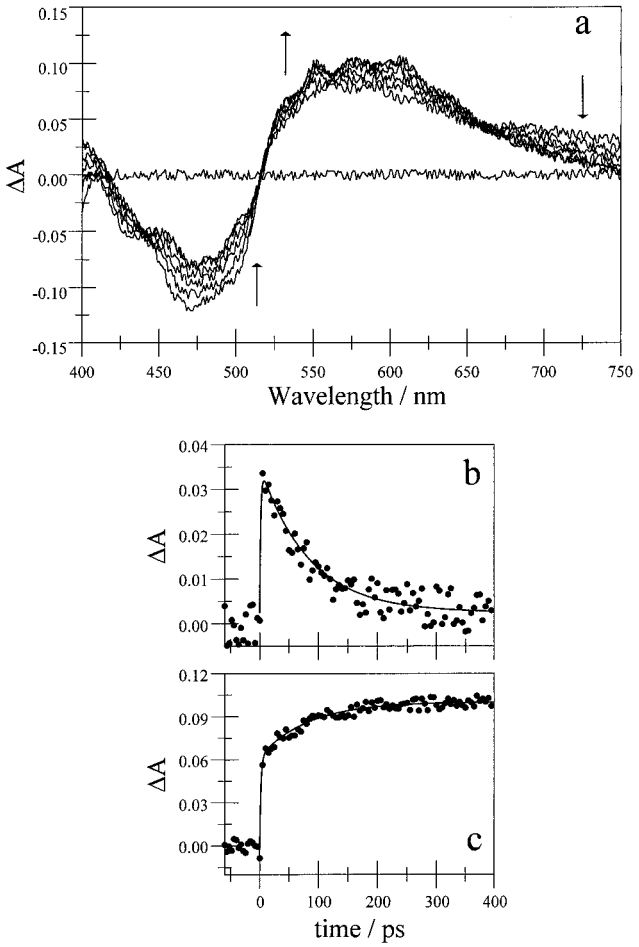

Figure 10. (a) Triplet differential absorption spectra recorded following laser excitation (fwhm = 0.35 ps; 565 nm) of RBA in deoxygenated acetonitrile. Spectra were recorded at delay times of 0, 10, 40, 80, 130, 200, 300, and 400 ps. Also shown are decay profiles recorded by overlaying transient spectra collected at different delay times for (b) 750 and (c) 600 nm. The solid lines drawn through the data points correspond to nonlinear least-squares fits to triplet lifetimes of (b) 85 ps and (c) 81 ps for the Ru(bpy) fragment.

collected at many different wavelengths. The derived value, together with that determined for RBABR, is given in Table 4 and compared to the spectroscopic energy gap. For these systems, the energy gap is too large to support reverse energy transfer from the connector to the Ru(bpy) fragment and because the energy gap greatly exceeds the combined reorganization energies, triplet energy transfer occurs well within the Marcus "inverted" region.[45]

Weak emission could be detected for OBA in deoxygenated acetonitrile at 20 °C which allows the determination of the triplet energy levels for the Os(bpy) fragment (Figure 8). This triplet lies at slightly lower energy than those in the corresponding naphthalene-based systems (Table 3), but the emission lifetime is unusually long and the differential triplet absorption spectrum is very similar to that recorded for the polytopic ligand (Figure 9). Such observations are consistent with thermal equilibration of the triplet states localized on Os(bpy) and on the anthracene-based connector,[2,5,46] as expected for an energy gap of ≈750 cm^{-1} (Table 4). This energy gap, which corresponds to an equilibrium constant of 40, indicates that the equilibrium distribution will contain only ≈2.5% of the triplet localized on the Os(bpy) fragment. Knowing that the inherent triplet lifetime for the anthracene-like triplet is (7.1 ± 0.6) μs, and allowing for α = 0.025, the inherent rate constant (k_O) for deactivation

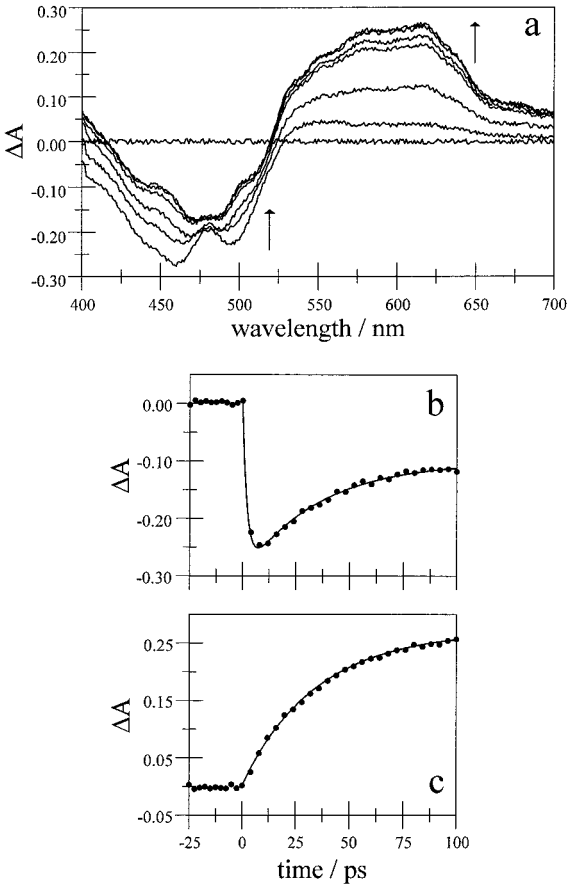

Figure 11. (a) Triplet differential absorption spectra recorded following laser excitation (fwhm = 0.35 ps; 600 nm) of OBA in deoxygenated acetonitrile. Spectra were recorded at delay times of 0, 5, 20, 40, 65, 90, and 100 ps. Also shown are decay profiles recorded by overlaying transient spectra collected at different delay times for (b) 450 and (c) 600 nm. The solid lines drawn through the data points correspond to nonlinear least-squares fits to triplet lifetimes of (b) 35 ps and (c) 33 ps for the Os(bpy) fragment.

of the Os(bpy) triplet can be estimated as being $\approx 9 \times 10^7$ s^{-1}. Thus, reverse energy transfer provides a substantial stabilization of the triplet state localized on the metal complex.

Excitation of OBA with a subpicosecond laser pulse at 600 nm, where the Os(bpy) fragment is the only absorbing species, generates the triplet state localized on the metal complex (Figure 11). The lifetime of this species, which is shortened because of energy transfer to the anthracene-based polytopic ligand, was found to be (33 ± 5) ps. Allowing for the equilibrium constant (K = 40) estimated from the spectroscopic energy levels, it becomes possible to derive rate constants for the forward and reverse energy-transfer steps (Table 4).

Comparison of the Rates of Intramolecular Triplet Energy Transfer. Several rate constants are now available for forward and reverse triplet energy transfer between a metal complex and an appended aromatic polycycle, together with the relevant energy gaps (Table 4). The rates are fast, especially those for reverse energy transfer where reaction is endergonic, but the separation distances are rather small and fixed throughout the series.[47] Each energy-transfer step is assumed to involve through-bond electron exchange in accordance with the Dexter mechanism[48,49] because the overlap integrals for Förster-type dipole−dipole energy transfer are negligible. It is useful in the context of designing improved prototypes to consider these rate constants in terms of the extent of electronic interaction between the reactants, this being a structural parameter. The simplest

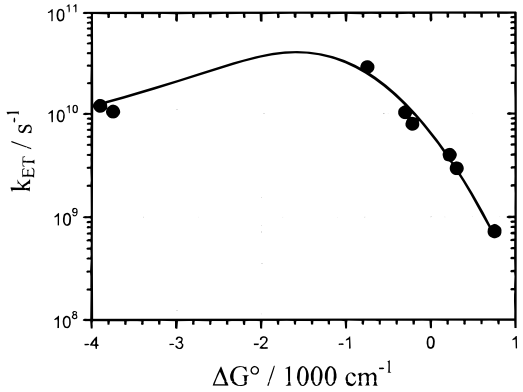

Figure 12. Correlation between the rate constant for electron exchange and the triplet energy gap. The solid line drawn through the data points corresponds to a nonlinear least-squares fit to eq 5 with the following averaged parameters: λ_T = 1460 cm^{-1}; S = 1.03; $\hbar\omega$ = 1400 cm^{-1}. Kinetic results are included for forward and reverse energy-transfer steps measured with RBN, RBNBR, RBA, RBABR, and OBA.

way to do so is to use averaged values for the reorganization energy and medium-frequency vibrational mode and to assume a constant value for the electronic coupling matrix element that describes through-bond electron exchange. In this case, variations in the rate are attributed entirely to the energy gap, and to have a reasonably large data set, it is further assumed that forward and reverse processes involve a common matrix element. As such, the rate constant for electron exchange (k_{ET}) can be expressed in terms of the Fermi golden rule:[12]

$$k_{ET} = \frac{2\pi}{\hbar} V_{DA}{}^2 \mathrm{FC}$$

$$\mathrm{FC} = \frac{1}{\sqrt{4\pi\lambda_T k_B T}} \sum_{n=0}^{\infty} \exp(-S)\left(\frac{S^n}{n!}\right) \exp(-\Delta G^*) \qquad (5)$$

$$\Delta G^* = \left(\frac{(\Delta G^\circ + \lambda_T + n\hbar\omega)^2}{4\lambda_T k_B T}\right)$$

Here, V_{DA} is the matrix element for electron exchange, λ_T is the total reorganization energy accompanying electron exchange, k_B is the Boltzmann constant, and T is the absolute temperature. The terms S and $\hbar\omega$ respectively refer to the averaged electron vibrational coupling constant and the averaged medium frequency vibrational mode coupled to the triplet states while ΔG° ($=-\Delta E_{TT}$) refers to the difference in triplet energy between the donor and acceptor. These various parameters, except V_{DA}, are available from analysis of the emission spectra recorded at ambient temperature after deconstruction into Gaussian-shaped components (Tables 2 and 3).[12] The parameters are reasonably consistent throughout the series, even for RBA and RBABR where there is little emission, such that appropriate averaged values can be obtained. An alternative procedure is to calculate the Franck−Condon factor for each pair of reactants from the individual parameters and obtain V_{DA} for each system.

As shown in Figure 12 there is a good correlation between the rate and energy gap throughout the series of compounds. The averaged matrix element (V_{DA} = 7.8 ± 0.8 cm^{-1}) is modest but in line with values reported for other triplet energy-transfer processes[50] and is somewhat higher than that (V_{DA} = 2.5 cm^{-1}) found[12] for bimolecular triplet energy transfer from Os(bpy) derivatives to anthracene. At the apex, the activationless rate constant is $\approx 5 \times 10^{10}$ s^{-1}. It is also apparent from Figure 12 that intramolecular energy transfer in RBA and RBABR shows

only a weak inverted effect.[45] Either quantum mechanical tunneling effects are important in these systems or triplet energy transfer occurs to an upper triplet localized on the anthracene-based connector, although our MO calculations locate the T_2 state at $\approx$23 000 cm^{-1}. If correct, this value would eliminate the T_2 level as a possible intermediate in the overall energy-transfer pathway. Inverted behavior has been observed for triplet energy transfer in both bimolecular[12b] and intramolecular cases[52,53] while related studies made with porphyrin-based clusters have provided strong evidence for through-bond interactions involving an alkynylene bridge.[54]

The alternative approach involves calculating[12,31] individual Franck−Condon factors from the spectroscopic data listed in Table 3 and estimating V_{DA} for each pair of reactants from the measured rate constants. The derived Franck−Condon factors span a fairly wide range (Table 4) and give an averaged V_{DA} of (9.5 $\pm$ 2.8) cm^{-1}. Thus, the two approaches are comparable but the latter method might be more useful in that it highlights those reactants where the electronic coupling differs from the norm. In the present case, it appears that V_{DA} for electron exchange between Ru(bpy) and the anthracene-like triplet is significantly smaller than that for the other reactants. In fact, it is the inclusion of data for RBA and RBABR that causes the V_{DA} obtained from the Marcus-type plot (Figure 12) to appear somewhat smaller than that estimated from the spectroscopic data.

Concluding Remarks

A prime motivation for this study is to identify how the nature of the central unit in a polyalkynylene connector might influence the rate of electron exchange along the molecular axis in mixed-metal Ru−Os binuclear complexes. Comparable energy-migration processes might take place between identical terminals in these symmetrical binuclear complexes, but such steps, being extremely difficult to identify experimentally, are ignored throughout the present investigation. On the basis of available information, it appears that a central phenylene unit will act as a partial insulator to inhibit through-bond electron exchange. Thus, at the triplet level, electron delocalization does not include the central phenylene unit due to a mismatch in energy and/or spatial distribution of local LUMOs. This situation seems appropriate for achieving relatively slow rates of intramolecular electron exchange. Replacing phenylene with naphthalene causes a substantial lowering of the triplet energy and LUMO energy of the connector, bringing both parameters closer to those associated with the terminal metal complexes. There is still a large energy gap between triplets localized on the connector and on the Os-based chromophores, but there are clear indications that orbitals on the bridge blend better with the chromophore. This effect is most obvious in the red-shifted emission spectra and in the reduction potentials. The triplet states localized on the corresponding Ru-based chromophores are almost isoenergetic with the naphthalene-containing connector. For Ru(terpy) this situation leads to a greatly prolonged triplet lifetime that might enable slow electron exchange to compete with nonradiative deactivation of the excited state. More significant is the finding that the connector triplet lies immediately below that of the Ru(bpy) terminal so that the two species enter into reversible triplet energy transfer at room temperature. This suggests that the connector triplet will operate as a real, rather than a virtual, intermediate in long-range electron-exchange events.

Replacing phenylene with anthracene pushes the connector triplet to very low energy such that triplet energy transfer from a terminal Ru(bpy) fragment falls well within the Marcus inverted region. Because of quantum mechanical tunneling, the rate remains fast but the resultant triplet state is of π,π^* character and does not involve the metal complex. In this case, the more interesting behavior is supplied by the Os(bpy)-based terminal, whose first-excited triplet state is situated at slightly higher energy than the connector triplet. This allows reversible triplet energy transfer to take place and provides a means for stabilizing the Os(bpy) triplet. The latter effect is nontrivial, leading to a 40-fold prolongation of the Os(bpy) triplet lifetime. Although the equilibrium lies well on the side of the anthracene-like triplet, this equilibration of the triplet states might facilitate electron exchange along the molecular axis in mixed-metal complexes, even if the final step is endergonic. In this case, the extended triplet lifetime of the Os(bpy) acceptor might favor secondary reactions (e.g., electron transfer) with adventitious reagents.

Acknowledgment. We thank the C.N.R.S., E.C.P.M., and the Royal Society of London for their financial support of this work. We are greatly endebted to Johnson-Matthey Ltd. for their generous loan of precious metal salts. The nanosecond laser flash photolysis studies were made at the Paterson Institute for Cancer Research, Manchester, England. We are most grateful to the staff of the FRRF-PICR for providing access to this equipment and to the E.E.C. for providing financial support to operate the facility and to defray travel expenses.

References and Notes

(1) Balzani, V.; Juris, A.; Venturi, M.; Campagna, S.; Serroni, S. *Chem. Rev.* **1996**, *96*, 759.
(2) Ford, W. E.; Rodgers, M. A. J. *J. Phys. Chem.* **1992**, *96*, 2917.
(3) Wilson, G. J.; Sasse, W. H. F.; Mau, A. W.-H. *Chem. Phys. Lett.* **1996**, *250*, 583.
(4) Wilson, G. J.; Launikonis, A.; Sasse, W. H. F.; Mau, A. W.-H. *J. Phys. Chem.* **1997**, *101*, 4860.
(5) Harriman, A.; Hissler, M.; Khatyr, A.; Ziessel, R. *Chem. Commun.* **1999**, 735.
(6) Hissler M.; Harriman, A.; Khatyr, A.; Ziessel, R. *Chem. Eur. J.* **1999**, *5*, 3366.
(7) Simon, J. A.; Curry, S. L.; Schmehl, R. H.; Schatz, T. R.; Piotrowiak, P.; Jin, X.; Thummel, R. P. *J. Am. Chem. Soc.* **1997**, *119*, 11012.
(8) Weinheimer, C.; Choi, Y.; Caldwell, T.; Gresham, P.; Olmsted, J., III *J. Photochem. Photobiol. A* **1994**, *78*, 119.
(9) Boyde, S.; Strouse, G. P.; Jones, W. E., Jr.; Meyer, T. J. *J. Am. Chem. Soc.* **1989**, *111*, 7448.
(10) Thornton, N. B.; Schanze, K. S. *New J. Chem.* **1996**, *20*, 791.
(11) Belser, P.; Dux, R.; Book, M.; De Cola, L.; Balzani, V. *Angew. Chem., Int. Ed. Engl.* **1995**, *34*, 595.
(12) Murtaza, Z.; Zipp, A. P.; Worl, L. A.; Graff, D. K.; Jones, W. E., Jr.; Bates, W. D.; Meyer, T. J. *J. Am. Chem. Soc.* **1991**, *113*, 5113. (b) Murtaza, Z.; Graff, D. K.; Zipp, A. P.; Worl, L. A.; Jones, W. E., Jr.; Bates, W. D.; Meyer, T. J. *J. Phys. Chem.* **1994**, *98*, 10504.
(13) Ryu, C. K.; Schmehl, R. H. *J. Phys. Chem.* **1989**, *93*, 7961. (b) Katayama, H.; Maruyama, S.; Ito, S.; Tsuji, Y.; Tsuchida, A.; Yamamoto, M. *J. Phys. Chem.* **1991**, *95*, 3480.
(14) To the best of our knowledge, the only relevant system for which rates of intramolecular triplet energy transfer free from diffusional effects are available is that described in ref 6.
(15) El-ghayoury, A.; Harriman, A.; Hissler, M.; Ziessel, R. *Coord. Chem. Rev.* **1998**, *178−180*, 1251.
(16) El-ghayoury, A.; Harriman, A.; Khatyr, A.; Ziessel, R. *Angew. Chem., Int. Ed.*, in press.
(17) Harriman, A.; Hissler, M.; Jost, P.; Wipff, G.; Ziessel, R. *J. Am. Chem. Soc.* **1999**, *121*, 14.
(18) El-ghayoury, A.; Ziessel, R. *Tetrahedron Lett.* **1997**, *38*, 2471.
(19) Sprintschnik, G.; Sprintschnik, H. W.; Kirsch, P. P.; Whitten, D. *J. Am. Chem. Soc.* **1977**, *99*, 4947.
(20) Kober, E. M.; Caspar, J. V.; Sullivan, B. P.; Meyer, T. J. *Inorg. Chem.* **1988**, *27*, 4587.
(21) Grosshenny, V.; Ziessel, R. *J. Organomet. Chem.* **1993**, *453*, C19.
(22) Pipes, D. W.; Meyer, T. J. *Inorg. Chem.* **1986**, *25*, 4042.
(23) Caspar, J. V.; Kober, E. M.; Sullivan, B. P.; Meyer, T. J. *J. Am. Chem. Soc.* **1982**, *104*, 630.
(24) Kober, E. M.; Marshall, J. L.; Dressick, W. J.; Sullivan, B. P.; Caspar, J. V.; Meyer, T. J. *Inorg. Chem.* **1985**, *24*, 2755.

(25) Lami, H.; Piermont, T. *Chem. Phys*. **1992**, *163*, 149.

(26) A preliminary account of triplet energy transfer in the Ru−Os mixed-metal complexes is given in ref 15.

(27) Harriman, A.; Hissler, M.; Ziessel, R. *Phys. Chem. Chem. Phys.* **1999**, *1*, 4203.

(28) Grosshenny, V.; Harriman, A.; Romero, F. M.; Ziessel, R. *J. Phys. Chem*. **1996**, *100*, 17472.

(29) Boyde, S.; Strouse, G. F.; Jones, W. E., Jr.; Meyer, T. J. *J. Am. Chem. Soc*. **1990**, *112*, 7395. (b) Downard, A. J.; Honey, G. E.; Phillips, L. F.; Steel, P. J. *Inorg. Chem*. **1991**, *30*, 2260. (c) Strouse, G. F.; Schoonover, J. R.; Duesing, R.; Boyde, S.; Jones, W. E., Jr.; Meyer, T. J. *Inorg. Chem*. **1995**, *34*, 473. (d) Benniston, A. C.; Goulle, V.; Harriman, A.; Lehn, J. M.; Marczinke, B. *J. Phys. Chem*. **1994**, *98*, 7798.

(30) Grosshenny, V.; Harriman, A.; Ziessel, R. *Angew. Chem., Int. Ed. Engl*. **1995**, *34*, 2705. (b) Benniston, A. C.; Harriman, A.; Grosshenny, V.; Ziessel, R. *New J. Chem*. **1997**, *21*, 405. (c) Harriman, A.; Hissler, M.; Ziessel, R.; De Cian, A.; Fischer, J. *J. Chem. Soc., Dalton Trans*. **1995**, 4067.

(31) Harriman, A.; Romero, F. M.; Ziessel, R.; Benniston, A. C. *J. Phys. Chem. A* **1999**, *103*, 5399.

(32) Benniston, A. C.; Grosshenny, V.; Harriman, A.; Ziessel, R. *Angew. Chem., Int. Ed. Engl*. **1994**, *33*, 1884. (b) Harriman, A.; Ziessel, R. *Chem. Commun*. **1996**, 1717. (c) Harriman, A.; Ziessel, R. *Coord. Chem. Rev*. **1998**, *171*, 331.

(33) Gould, I. R.; Noukakis, D.; Gomez-Jahn, L.; Young, R. H.; Goodman, J. L.; Farid, S. *Chem. Phys*. **1993**, *176*, 439.

(34) Cortés, J.; Heitele, H.; Jortner, J. *J. Phys. Chem*. **1994**, *98*, 2527.

(35) Striles, M.; Cline Love, L. J. *Anal. Chem*. **1980**, *52*, 1559.

(36) Englman, R.; Jortner, J. *Mol. Phys*. **1970**, *18*, 145.

(37) Bryne, J. P.; McCoy, E. Y.; Ross, I. G. *Aust. J. Chem*. **1965**, *18*, 1589.

(38) Beer, M. *J. Chem. Phys*. **1956**, *25*, 745. (b) Nagano, Y.; Ikoma, T.; Akiyama, K.; Tero-Kubota, S. *J. Phys. Chem*. **1998**, *102*, 5769.

(39) Molecular-orbital calculations made for the optimized conformations of the polytopic ligands indicate triplet energies of 21 500 and 22 200 cm^{-1}, respectively, for BPB and TPT, after first optimizing the calculation by reference to diphenylacetylene (see ref 38). Similar calculations made for BNB and TNT, respectively, give triplet energies of 16 000 and 16 500 cm^{-1}. The calculated triplet energy of BAB is 11 900 cm^{-1}.

(40) Grosshenny, V.; Harriman, A.; Hissler, M.; Ziessel, R. *J. Chem. Soc., Faraday Trans*. **1996**, *92*, 2223.

(41) El-ghayoury, A.; Harriman, A.; Hissler, M.; Ziessel, R. *Angew. Chem., Int. Ed*. **1998**, *37*, 1717.

(42) This effect can be seen in both cyclic voltammetry and infrared spectroscopy where the nature of the central polycycle affects both E_{RED}-(1) and $\nu_{C\equiv C}$. The cyclic voltammograms further indicate that the central aromatic unit itself can be reduced in the case of naphthalene and anthracene but not in the case of phenylene.

(43) Murov, S. L. In *Handbook of Photochemistry*; Marcel Dekker Inc.: New York, 1973.

(44) The equilibrium constant (K) can be estimated as $\Delta E = -RT \ln(K)$ where ΔE refers to the difference in energy between triplet states localized on the connector and on the terminal metal complex. The fractional contribution of triplets localized on the metal complex in the equilibrium mixture can be calculated as $\alpha = (1/(1 + K))$ so that the rate constants for forward ($k_{ET}^{F} = (1 - \alpha)/\tau_S$) and reverse ($k_{ET}^{R} = \alpha/\tau_S$) energy-transfer steps can be derived from the lifetime of the shorter-lived component. Similar calculations made for RTN ($\Delta E = 1500$ cm^{-1}; $\alpha = 0.999$) and OBN ($\Delta E = 2715$ cm^{-1}; $\alpha = 1.0$) indicate that reverse energy transfer is unlikely to compete with inherent decay of the triplet state localized on the metal complex.

(45) Marcus, R. A.; Sutin, N. *Biochim. Biophys. Acta* **1985**, *811*, 265.

(46) El-ghayoury, A.; Harriman, A.; Khatyr, A.; Ziessel, R., *Chem. Commun*. **1999**, 2027.

(47) Molecular mechanics simulations based on the AMBER force field indicate that the metal−metal separation in the binuclear complexes is ≈20 Å. The edge-to-edge distance between the pyridine ring and the central polycycle is only 3.8 Å while the distance separating the metal center from the edge of the central polycycle is 8.5 Å. The distance between the metal center and the center of the polycycle is 9.8 Å. The computer simulations further indicate that the molecule is not linear but is bent about the connector. Thus, for RTNTR the out-of-plane bending of the connector is ≈34° while the [calculated] activation energy for rotation around the connector is 3 kcal mol^{-1}. These values seem reasonable in light of the detailed NMR studies made with ethynylene-bridged bis-porphyrins (see ref 47b). (b) Bothner-By, A. A.; Dadok, J.; Johnson, T. E.; Lindsey, J. S. *J. Phys. Chem.* **1996**, *100*, 17551.

(48) Dexter, D. L. *J. Chem. Phys*. **1953**, *21*, 836.

(49) Razi Naqvi, K.; Steel, C. *Spectrosc. Lett*. **1993**, *26*, 1761.

(50) According to the nature of the bridge and the theoretical treatment used to analyze the kinetic data, values for V_{DA} ranging between 0.4 and 60 cm^{-1} have been reported for electron-exchange reactions involving "Ru(bpy)" fragments. For further details see refs 6, 12, 30a, 31, and 51 and publications quoted therein.

(51) Liang, L. Y.; Baba, A. I.; Kim, W. Y.; Atherton, S. J.; Schmehl, R. H. *J. Phys. Chem*. **1996**, *100*, 18408. (b) Shaw, J. R.; Sadler, G. S.; Wacholtz, W. F.; Ryu, C. K.; Schmehl, R. H. *New J. Chem*. **1996**, *20*, 749.

(52) Sigman, M. E.; Closs, G. L. *J. Phys. Chem*. **1991**, *95*, 5012.

(53) MacQueen, D. B.; Eyler, J. R.; Schanze, K. S. *J. Am. Chem. Soc*. **1992**, *114*, 1997.

(54) Strachen, J.-P.; Gentemann, S.; Seth, J.; Kalsbeck, W. A.; Lindsey, J. S.; Holten, D.; Bocian, D. F. *J. Am. Chem. Soc*., **1997**, *119*, 11191. (b) Li, F.; Gentemann, S.; Kalsbeck, W. A.; Seth, J.; Lindsey, J. S.; Holten, D.; Bocian, D. F. *J. Mater. Chem*. **1997**, *7*, 1245. (c) Van Patten, P. G.; Shreve, A. P.; Lindsey, J. S.; Donohue, R. J. *J. Phys. Chem. B* **1998**, *102*, 4209.